



Characterization and Surface Modification of Gold Nanorods in Colloidal Solutions

Anna Gibalova

Moscow State University, Faculty of Chemistry

Supervisor: Dr. Irina Lokteva

September 6, 2017

Contents

1. Introduction.....	2
2. Determination of concentration of Au nanorod solutions.....	3
2.1 Experimental part.....	3
2.2 Results and discussion.....	3
3. PEGylation of the Au nanorods	5
3.1 Experimental part.....	6
3.1.1 PEGylation	6
3.1.2 Interaction of AuNRs with KCl solution	7
3.1.3 Solvent exchange.....	7
3.1.4 Etching experiments.....	7
3.2 Results and discussion.....	7
3.2.1 Interaction of Au NRs with KCl solution	7
3.2.2 Solvent exchange.....	10
3.2.3 Etching procedure	11
4. Characterization of Au NRs with TEM and DLS	11
4.1 Experimental part.....	11
4.1.1 TEM.....	11
4.1.2 DLS measurements.....	12
4.2 Results, discussion and data processing.....	12
4.2.1 TEM image analysis	12
4.2.2 MP DLS.....	16
5. Purification procedure of non-monodisperse Au nanorod sample	19
5.1 Experimental part.....	20
5.2 Results and discussion.....	20
6. Conclusions.....	23
7. Literature references.....	24
8. Acknowledgments	26

1. Introduction

This report summarizes the results of my summer research project which was carried out in the group of Coherent X-ray Scattering in the Photon Science department (FS-CXS) from July to September 2017.

Topic of my summer research project at DESY was associated with characterization and post-synthetic processing of gold nanorods (Au NRs). Those particles have received a lot of attention because of a number of promising properties that may allow using them in a number of applications, such as solar harvesting, photovoltaics, surface enhanced spectroscopies, sensing, and therapy.

Even though a lot of reliable methods for the synthesis of gold nanorods have been developed up to now still a lot of challenges are left to produce monodisperse nanorods with desired size/aspect ratio and to ensure the stability of the stored colloidal sample for a long time. In order to provide the aforementioned stability one should work on the problem of nanorod surface chemistry which involves the surface modification of as-synthesized particles. In this project we carried out the ligand exchange of CTAB(cetyltrimethylammonium bromide)-stabilized Au NRs with PEG-SH (poly(ethylene glycol) thiol) which is widely used because it can provide biocompatibility and stability of Au NR solution at once. Sometimes synthesized samples may be not monodisperse enough and one would need to think about purifying procedure from undesirable shapes. In this work we applied the purification of Au nanorod colloids via depletion forces using addition of concentrated CTAB solution. For the post-synthetic characterization of Au NRs we used methods of UV-VIS-NIR spectroscopy, TEM (Transmission Electron Microscopy) and DLS (Dynamic Light Scattering). Additionally, the part of my work was to develop the algorithm for the analysis of TEM images which is more complicated for anisotropic particles.

2. Determination of concentration of Au nanorod solutions

2.1 Experimental part

The sample under study was IL 26, which was synthesized previously according to [1], method 1e, after synthesis the particles were centrifuged at 7000 rpm for 30 min and redissolved in 10 ml of water.

The concentration of Au NRs was studied by means of UV-VIS-NIR spectroscopy. The absorption spectra were measured using the CARY 5000 spectrophotometer in cuvette with 10mm path length. The concentration was determined by two methods.

The first method involves the measurement of the absorbance of a diluted NR solution at 400 nm, from which the reduction yield of gold can be precisely estimated regardless of the size and shape of nanoparticles [2]. This wavelength is chosen because below 400 nm the absorbance is influenced by organic substances and above the absorbance is influenced by the LSPR (Localized Surface Plasmon Resonance) of the gold nanorods. Thus, an absorbance at 400 nm of 1.2 corresponds to $[\text{Au}^0] = 0.5 \text{ mM}$.

In the second method the concentration is determined from the Lambert-Beer law, where the extinction coefficient at the LSPR wavelength (837 nm in case of the sample IL26) is taken from literature [3]. Since the extinction coefficient depends on the size of particles it is crucial to find the reliable literature values corresponding to the particular sample.

2.2 Results and discussion

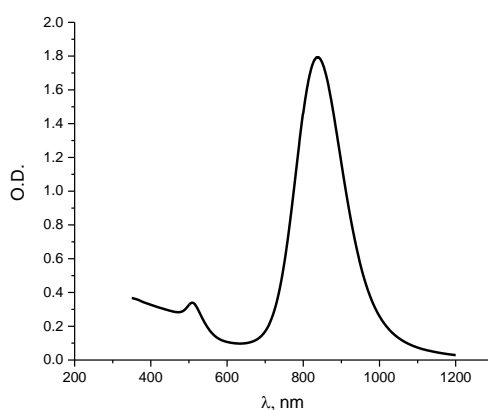


Figure 1 . UV-VIS-NIR spectrum of IL26 sample.

The absorption spectrum of IL26 is shown in Figure 1, where optical density at 400 nm is 0.327 and at 837 nm is 1.79. According to the first method, determination of $[\text{Au}^0]$ concentration in the cuvette was $0.327/2.4 = 0.136 \text{ mM}$ and 0.0137 M in the bulk solution.

Even though the precise determination of extinction coefficients for Au nanorods seems to be a difficult task several groups have reported about that. In [3] several extinction coefficients for a number of samples of Au nanorods with different shapes and sizes at the LSPR wavelength were calculated using the Lambert-Beer law and the gold concentration determined by ICP-MS (Inductively coupled plasma mass spectrometry) analysis. Extinction coefficients for Au NRs at the wavelength of the longitudinal surface plasmon resonance can be considered as a function of effective radius, $R_{eff} = \sqrt[3]{\left(\frac{3V}{4\pi}\right)}$ (where R_{eff} is the radius of a sphere having a volume, V , equal to that of the nanorod) [4]. Proceeding from this assumption we have calculated R_{eff} for the sample IL26 from the results of TEM image analysis (which can be found below).

The average length and diameter from the TEM were found to be 74 and 20 nanometers respectively. If we consider our particles as cylinders with two hemispheres at the ends (Fig.2) we can calculate the average volume of the particle from the data obtained from TEM ($d = 2r$):



Figure 2. Schematical representation of an Au nanorod.

$$V = V_{cylinder} + V_{sphere} = \pi \left(\frac{d}{2}\right)^2 (l - d) + 2 * \frac{4}{6}\pi \left(\frac{d}{2}\right)^3 = 21143 \text{ nm}^3$$

So that R_{eff} is $\sqrt[3]{\left(\frac{3V}{4\pi}\right)} = 17.16 \text{ nm}$

According to [3] the closest value of extinction coefficient on LSPR wavelength for this effective radius is $1.13 \cdot 10^{10} \text{ L} \cdot \text{mol}^{-1} \cdot \text{cm}^{-1}$. Optical density at the LSPR wavelength (837 nm) for our sample is 1.79 so we obtain the concentration in our sample to be $1.58 \cdot 10^{-10} \text{ M}$ (or 0.158 nM) of Au nanorods in our sample and 15.96 nM in the bulk solution.

To compare the obtained results from both methods we should convert the concentration of $[\text{Au}^0]$ from the first method to the concentration of nanorods using the following equation:

$$c(\text{Au}_{NR}) = \frac{[\text{Au}^0] * M(\text{Au})}{V(\text{Nanorod}) * \rho(\text{Au}) * N_A} = 0.11 \text{ nM (in the cuvette)}$$

and 11 nM in the bulk solution. Results of the particle concentration obtained by two different samples do not differ significantly (less than by 1.5 times), which is still rather acceptable for this accuracy level. To improve the results one should take into account the non-ideal shape of the particles and probably find the exact extinction coefficient value for the calculated R_{eff} .

3. PEGylation of the Au nanorods

The biggest part of my experimental work was study of surface coverage of IL26 particles to improve their stability. To enable the further use of synthesized gold nanorods, control of their surface chemistry is necessary. Typical surfactant used for synthesis of Au nanorods is cetyltrimethylammonium bromide ($C_{19}H_{42}BrN$, CTAB) which appears to be good in the synthesis procedure but not very reliable in the question of long storage. So the obtained solutions usually undergo a ligand exchange procedure. However, the ligand exchange of CTAB may be much more challenging than, for example, exchange of citrate, which is widely used in synthesis of spherical Au nanoparticles, and at the same time necessary both for medical purposes and many other scientific applications. CTAB forms a densely packed bilayer [5] at the Au NR surface that requires a sufficiently high concentration of unbound CTAB in solution to provide effective stabilization of the Au NRs. Thus, it can be really difficult to remove the surfactant (especially the surface bound) without affecting the stability of the colloidal suspension. Some successful results with use of some additives, e.g. ethanol [6] or chloroform [7] to extract CTAB, which result in sufficient stabilization of the nanoparticles are reported.

Usually CTAB is exchanged for polymers to stabilize the gold nanoparticles and the most important type of them is poly(ethylene glycol)- (PEG-) thiols, which can provide biocompatibility and stability at once. Process of ligand exchange in this case is usually called PEGylation. However, even after this process considerable amounts of CTAB may remain on the nanorod surface, which rises doubts about the colloidal stability [8].

To study the effect of conditions and repeatability of surface modification with PEG-SH we used different methods for the PEGylation of the IL26 sample. Thus we applied simple mixing of solutions (round 1) or preliminary CTAB removal with chloroform extraction (rounds 2-4), after which the success of the ligand exchange was tested using different methods.

A plenty of methods to detect the occurred ligand exchange have been developed up to now. Typically FTIR-spectroscopy and X-ray photoelectron spectroscopy are used to determine the loading of PEG-SH on nanorods, as it is easy to find the S-Au vibration in spectra. However some easier and cheaper techniques can also be used for the study of surface functionalization of AuNRs with PEG-SH, for example, by testing their colloidal stability in water upon addition of NaCl or KCl solutions [8,9]. It is also known that PEG-SH modified nanorods are also soluble in organic solvents (e.g. in comparison to CTAB-capped nanorods which are only soluble in water) [10]. Moreover, some other techniques can be applied to check the success of the PEGylation, for example, the etching procedure with KCN [11] or $FeCl_3$ [12] where the PEG-coated Au NRs exhibit stability upon etching. The results of these experiments are explained below.

3.1 Experimental part

3.1.1 PEGylation

For the ligand exchange with PEG we used the sample IL26 Au nanorods. Methoxy-PEG-SH ($\text{CH}_3\text{O-PEG-SH}$) with molecular weight of 800 Da was purchased from Rapp Polymere. PEG-SH was dissolved in water and the concentration of the obtained solution was 100 mg/ml. Conditions of PEGylation are listed in the Table 1.

Table 1. Conditions of PEGylation of IL 26 Au nanorods.

Sample name	V (IL26-AuNRs solution), ml	V (PEG solution), ml
Round 1		
A1	1	1
A3	0.250	0.5
A4	1.5	1
A5	1.5	1.5
Round 2		
S1	0.3	0.5*3
S2	0.3	0.5*3
Round 3		
O1	0.2	0.2*3
O2	0.2	0.033*3
O3	0.2	0.02*3
O4	0.2	0.067*3
O5	0.2	0.133*3
O6	0.2	0.01*3
Round 4		
T1	0.15	0.25*3

Round 1

Samples A1, A3 were mixed without purification of the stock IL26 Au NRs solution and left stirred overnight.

Samples A4, A5 were centrifuged and redispersed in water 2 times before adding PEG solution and were left stirred overnight. Sample A4 was solid on the walls of the tube after centrifugation, sample A5 was redispersed in water after centrifugation, but the particles formed big aggregates in water before addition of PEG.

Round 2

Sample S1 was washed 3 times with chloroform before adding PEG; S2 was washed 3 times with chloroform after adding PEG. Addition of PEG was followed by centrifugation and it was repeated 2 times, after that the particles were redispersed in PEG solution (S1) or in chloroform (S2).

Round 3

All samples were washed 3 times with chloroform (3*0.5ml) before adding PEG solutions. Addition of PEG was followed by centrifugation and it was repeated 2 times, then particles were redispersed in PEG solution.

Round 4

The same procedure as in round 3.

3.1.2 Interaction of Au NRs with KCl solution

KCl was obtained from Riedel de Haen. Two concentrations of 0.1 and 1 M solution were used in this study.

The degradation process or stability of Au NR solutions were monitored by the UV-VIS-NIR spectroscopy upon addition of KCL solutions. For this, 20 μ l of stock Au NRs solution (IL26) were mixed with 1000 μ l of KCl solution. Spectra were recorded with the UV-VIS-NIR CARY 5000 spectrophotometer in the range of 1200-350 nm.

3.1.3 Solvent exchange

Chloroform was obtained from Sigma Aldrich. A little amount of sample dissolved in water was centrifuged for 15 minutes at 7000 rpm, water supernatant was removed and chloroform was added followed by vigorous shaking.

3.1.4 Etching experiments

Etching experiments were done according to (7). Typically, the solution of Au nanorods (IL26-stock, A4 and A1), was diluted to a final concentration of CTAB of approximately 2 mM. Then, 100 μ L of 0.6 M FeCl_3 was added to 1 mL of the above solution. The products at different reaction times were spun down, redispersed in ultrapure water and measured by the absorption spectrophotometer.

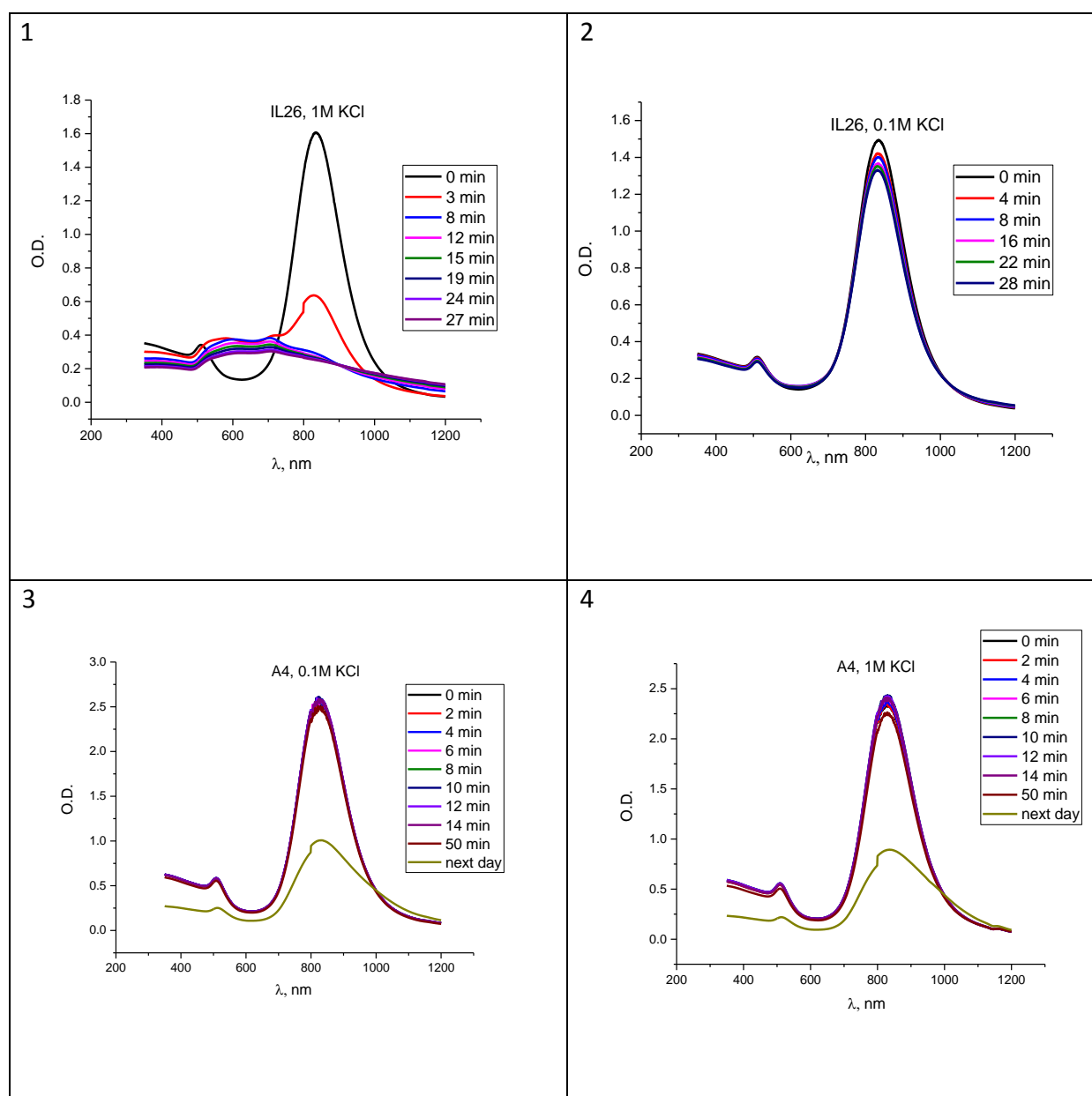
3.2 Results and discussion

3.2.1 Interaction of Au NRs with KCl solution

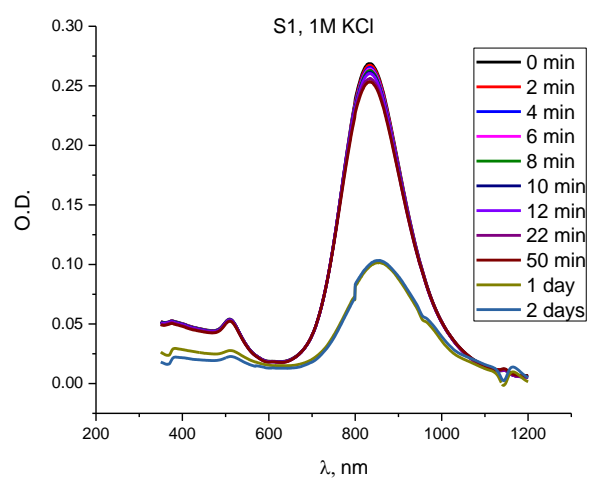
As it was already mentioned before, the efficiency of the surface functionalization of Au NRs with PEG-SH can be investigated by testing their colloidal stability in aqueous solution at

different NaCl or KCl concentrations [9]. In [9] the decrease of the longitudinal surface plasmon (LSPR) peak intensity of the Au NRs capped with either CTAB or PEG-SH was observed upon increasing the NaCl concentration (compared to the absorption intensity of the LSPR before NaCl addition). In the case of CTAB-capped Au NRs, the rate of LSPR peak depletion, was almost six times higher than that of PEG-SH-capped Au NRs with increasing the concentration of NaCl in the Au NR dispersion (according to the slope of the LSPA peak intensity against different NaCl concentrations). This implies that the stability of PEG-SH-modified Au NRs against aggregation is much higher than that of CTAB-capped Au NRs and, as a consequence, the toxicity effect related to massive precipitation could be minimized for PEG-SH-capped Au NRs in biomedical applications.

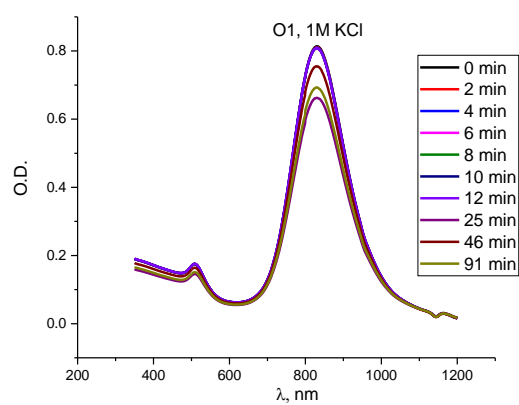
The degradation of Au NR solutions was monitored by absorption spectroscopy (Fig. 3) The concentration of Au NRs was measured by UV-VIS-NIR spectroscopy and ratio of KCl to Au was adjusted to be the same in all cases.



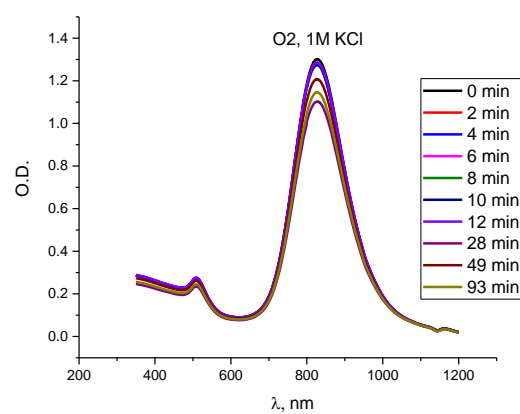
5



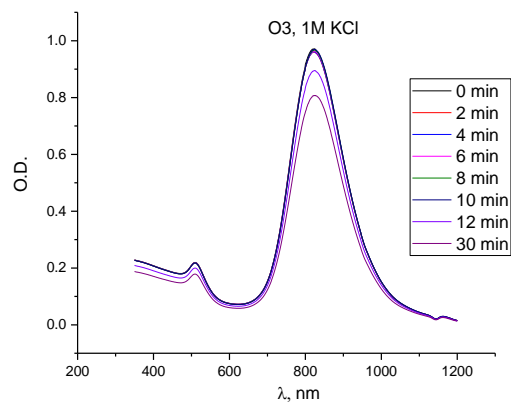
6



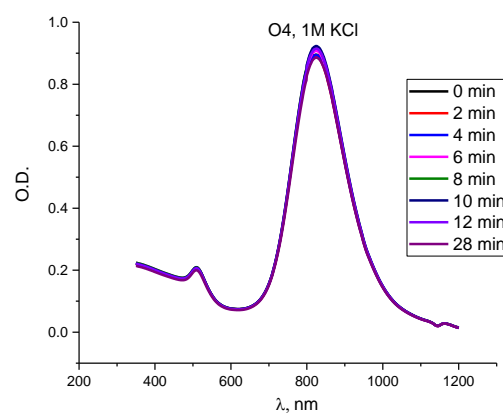
7



8



9



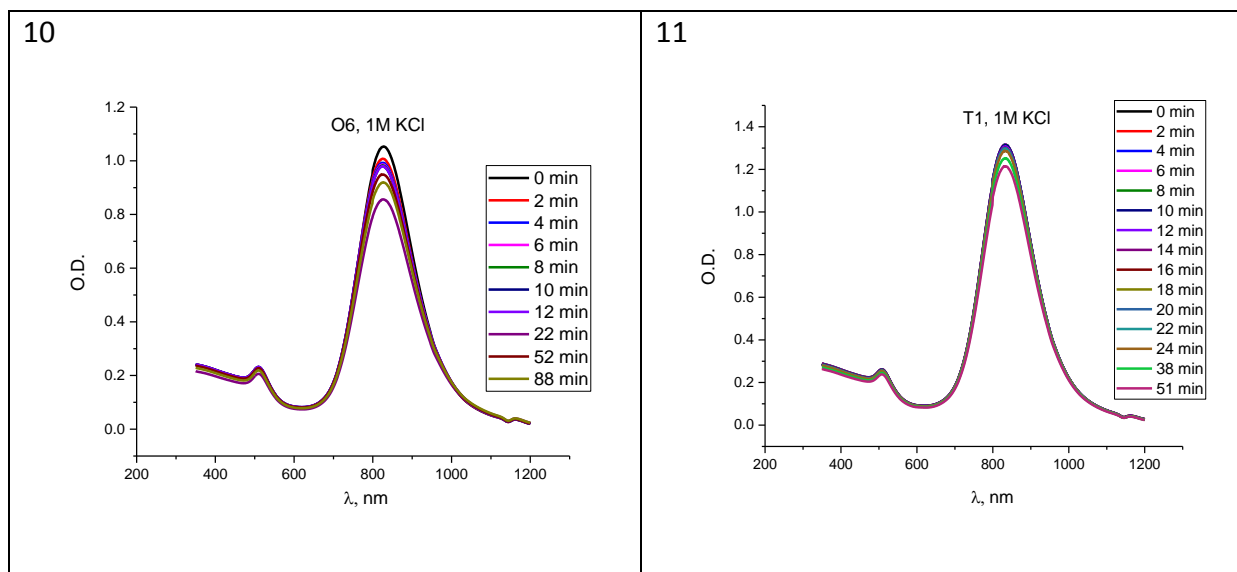


Figure 3. Absorption spectra of different Au nanorod samples upon addition of KCl

Plot 1 (Fig.3) represents the degradation process of IL26-stock solution with 1 M KCl solution. It can be seen, that the absorbance at 837 nm decreases rapidly whereas the absorbance at 900-1000 nm increases what refers to aggregate formation and destruction of the colloidal system; similar results were obtained with 0.1 M KCl solution (plot 2) where the degradation occurred much slower due to lower KCl concentration. At the same time the spectra 3-5 (PEGylated Au NRs) show almost no decay of the samples A4 and S1 during the observation period: the position of the LSPR peak does not change after ligand exchange with PEG, which indicates successful ligand modification procedure; only after one day the colloidal system becomes unstable. After these results several experiments were conducted with lower PEG concentrations to determine the minimum concentration of PEG necessary for successful ligand exchange. Unfortunately, nearly all samples were not stable enough: spectra 6-8 and 10-11 show slow decay during the observation time, which was not observed for the samples A4, S1 (plots 3-5); only sample O4 (plot 9) demonstrates nearly the same stability. After this failure one more attempt was made to repeat the successful ligand exchange with the same amount of PEG-SH as in the sample 5. Unfortunately, the stability of the sample also decreased in comparison to the S1 sample, so we came to the conclusion that the solution of PEG-SH degraded. It is well-known that thiol water solutions are not very stable and decay rapidly [13] but in our case it was necessary to dissolve all the PEG at once in order to get the precise concentration.

3.2.2 Solvent exchange

Solvent exchange procedure was done to the particles that appeared to be stable in a KCl addition experiment, that are A4 and S1. Both samples redispersed readily in chloroform and formed a transparent solution.

3.2.3 Etching procedure

Unfortunately, the etching experiments cannot be considered as successful. The procedure was done to samples IL26 and A4 and different results were obtained. Sample A4 decayed very fast: after 30 minutes of incubation the solution became green (typical color of Fe^{2+} compounds in water) and no trace of Au nanoparticles was found in the UV-VIS spectra. On the other hand, IL26 showed almost no decay: spectra remained unaltered. These results may indicate that the concentration of Au nanorod samples was extremely different in these two experiments, so that the reaction in the case of A4 happened too quickly and in the case of IL 26 was too slow to observe.

In the Table 2 the observations of PEGylated Au NR samples upon addition of KCl and solvent exchange with chloroform are summarized.

Table 2. Results of PEGylation experiments.

A1	Aggregation occurred
A3	Aggregation occurred
A4	Stable in KCl solution
A5	Aggregation occurred
S1	Stable in KCl solution
S2	Stable CHCl_3 solution; no redispersion in water
O1	Slow decay in KCl solution
O2	Slow decay in KCl solution
O3	Slow decay in KCl solution
O4	Very slow decay in KCl solution: almost stable sample
O5	Sample was lost by spilling
O6	Slow decay in KCl solution
T1	Slow decay in KCl solution

(KCl solutions refers to both 1M and 0.1M concentrations).

4. Characterization of Au NRs with TEM and DLS

4.1 Experimental part

4.1.1 TEM

TEM measurements were performed at the University of Hamburg using Phillips CM 300 transmission electron microscope with a 300 kV accelerating voltage. For TEM imaging, the drop containing nanoparticles was dried on a special grid. Image processing was made using ImageJ software (see below).

4.1.2 DLS measurements

Multipolarization (MP) DLS measurements were carried out at the University of Hamburg. A laser with $\lambda = 520$ nm was used as a light source. The DLS set up included a Glan-Thompson prism to adjust the polarization angle. A fast real-time software correlator based on a multitaup algorithm ALV/LSE-5003 was used for ACF (autocorrelation functions) calculations. Prior to the MP DLS measurements, all samples were diluted. During MP DLS measurements, intensity ACFs were measured for the scattering angles of 75° and 90°; for each scattering angle, measurements were performed for several values of the polarization angle. The most often used set of angle values included 0°, 45°, 60°, 70°, 80° and 90°. Analysis of obtained results was done by Matlab using the code from [14] with corrected parameters for our case.

4.2 Results, discussion and data processing

4.2.1 TEM image analysis

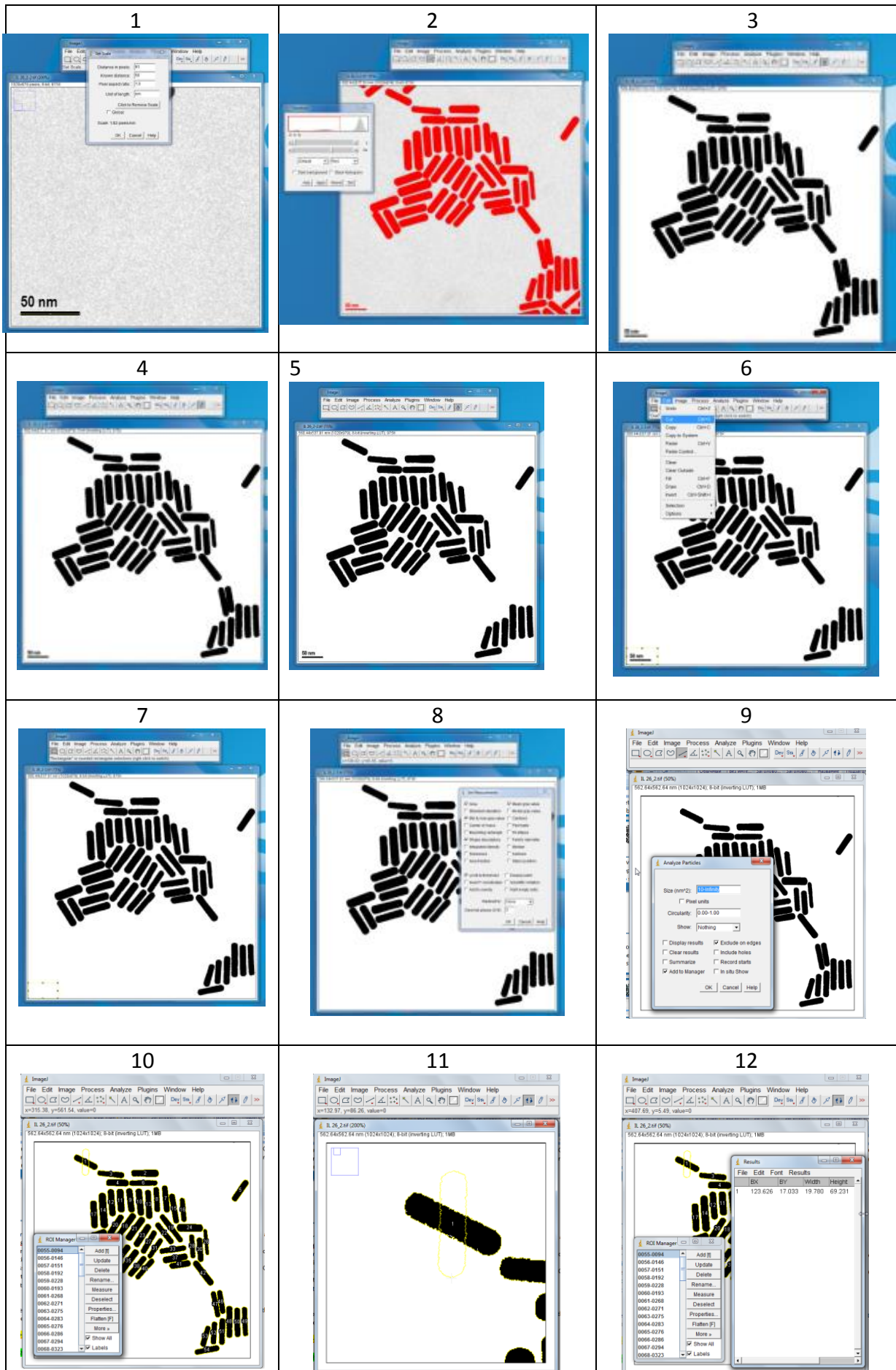
Obtained images were analyzed using ImageJ software [15]. ImageJ is an open source Java-based image processing program developed at the National Institutes of Health and it is widely used for the analyzing of TEM images of nano- and macroparticles. The automatic image analysis is not trivial, especially for nonspherical particles due to difficulties in applying the correct threshold in case of particle overlapping and various parameters describing the dimensions of non-spherical particles. Below a semi-automatic method that I developed for Au NRs in the frame of this summer project.

The semi-automatic algorithm for nanorod analysis using with ImageJ

1. Upload an image file of interest by pressing down File -> Open -> Choose the path.
2. Select a region of interest by applying the selection tool and drawing a box around the area of interest with particles you want to analyze. Then select Image -> Crop
3. Set appropriate realistic metrics considering the preliminary designated scale:
 - i. Choose "Straight Line" in the fast-access panel
 - ii. Hold down the shift key and draw a straight line along the length of the scale bar of the image being as precise as possible
 - iii. Change the data in "Known distance" and "Unit of length" strings to represented scale values in the following dialog window: Analyze -> Set Scale (Fig. 4.1)
4. Apply the proposed threshold-recognition tool: Image -> Adjust -> Threshold. Adjust the threshold by sliding the bars so that only the particles you wish to analyze are selected. You may need to slide the top bar all the way to the left and then adjust the lower bar to do this, then choose Apply. This operation is relevant because of noticeable contrast between each "particle"-shade and the background (Fig.4.2)

5. Choose "Flood Fill" tool in the fast-access panel and apply it on every edge-intersecting particle in order to avoid wrong data in the set of measurements(Fig. 4.3)
6. If processed picture contains cross-intersecting particles it is necessary to separate them manually and there are three ways of doing it, the choice depends on the depth of intersection:
 - Using Erode-Dilute function
 - i. Apply "Erode" tool to make the whole correction more visual-friendly: Process -> Binary -> Erode
 - ii. Use "Pencil" and remove every existing intersection between particles (Keep in mind that ImageJ tends to interpret "corner-touched" pixels as intersection).
 - iii. Apply "Dilute" tool to return at the initial state: Process -> Binary -> Dilute.
 - Using only the "Pencil" tool for removing all existing intersections and drawing a visible border between the particles (if it is obvious where it must be) (Fig. 4.4)
 - Using the "Flood Fill" tool for deleting the intersecting particles (if the particles in the aggregate are impossible to be distinguished as single particles) (Fig. 4.5)
7. Check for reinstalled intersections.
8. Cut and fill the scale bar with consecutive application of Freehand (or any other type of selection) tool, Edit -> Cut and Edit -> Fill, respectively (Fig. 4.6, 4.7)
9. Set measurements to the ones you need: Analyze -> Set Measurements. Strictly suggested to place a benchmark on "Limit to threshold" (Fig. 4.8)
10. Eventually, start the actual analysis: Analyze -> Analyze Particles. Make the "Add to Manager" benchmark active for granting yourself an opportunity to manipulate with distinguishable ROIs. For more detailed representation "Show: Overlay" is recommended to make the numeration of particles visual and to see if there are any intersections left (Fig. 4.9)
11. By means of "Selection Rotator" (it might be useful to arrange tool on the quick-access interface) and parcing through the ROI manager accomplish the following:
 - By mouse-clicking on ROI-selected line and appropriate slide of controller achieve the "vertical" particle position (Fig. 4.10, 4.11)
 - Press key "M" to make a measurement, the program would automatically update the current ROI's position (Fig 4.12)
 - Continue actions 1 and 2 for every single selected line (Fig 4.13)
12. Export just acquired data in any convenient file extension format. The typical data analysis implies the Excel's math engine then .xls format stands as vital and common choice (Fig. 4.14).

Different steps of the particle analysis procedure are summarized in Figure 4.



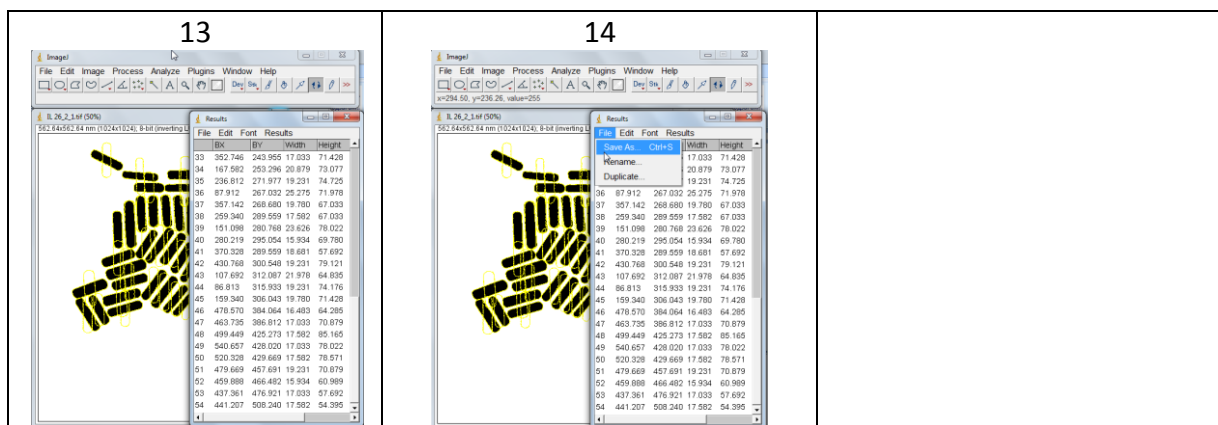


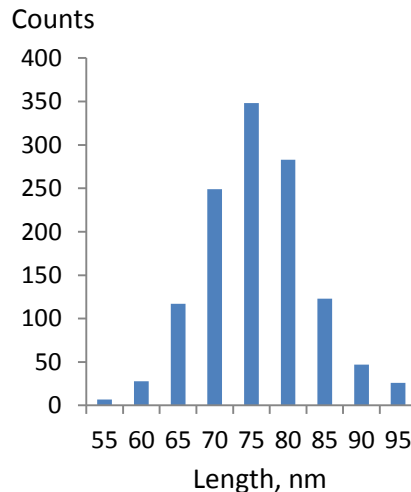
Figure 4. Illustrations to the semi-automatic ImageJ particle analyzing procedure

After ImageJ's procedure several .xls files had been extracted. Each of them contained width and length characteristics based on every outprocessed particle with total amount of 1237, respectively. Finally, every piece of data was united in one .xls file in order to make calculations more precise. For actual statistical data analysis appropriate Excel package was utilized, in particular, for each parameter descriptive statistics and histogram have been obtained. Aforementioned results are represented below:

➤ Particle length

Bins	Counts
55	7
60	28
65	117
70	249
75	348
80	283
85	123
90	47
95	26
Else	9

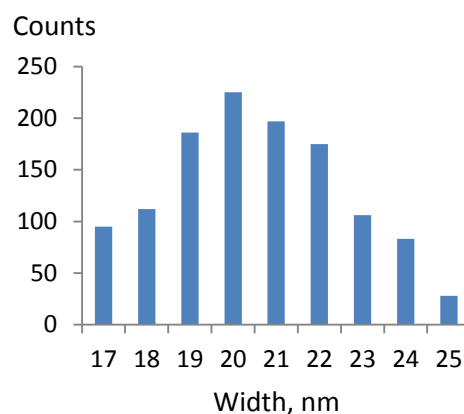
Statistics	
Mean	73.55
Standard error	0.22
Median	73.12
SD	7.83
Dispersion	61.27



➤ Particle width

Bins	Counts
17	95
18	112
19	186
20	225
21	197
22	175
23	106
24	83
25	28
Else	30

Statistics	
Mean	20.14
Standard error	0.075
Median	20.245
SD	2.65
Dispersion	7.02



Indeed, it seems obvious that qualitatively almost every processed particle might be recognized as a “rod”-shaped one. Furthermore, the average particle is 20 nm in width and 74 nm in length with 2.6 nm and 7.8 nm standard deviations, respectively (with 95% confidence interval). Thus, it could be concluded that set of analyzed data has less than 15% “relative” deviation near the corresponding mean value for each parameter. This fact can be designated as an evidence of narrow size distribution for both dimensions and particles themselves.

4.2.2 MP DLS

Dynamic light scattering (DLS) technique allows for determination of the particles sizes and their distributions in a colloidal solution. Presence of a depolarized component in the light-scattering signal enables to access both the translational and rotational diffusion of anisotropic particles, such as nanorods. As a result, depolarized dynamic light scattering can be used not just to obtain the hydrodynamic radius of the equivalent sphere but also to determine the actual length and diameter of diffusing nanorods. By considering nanoparticle Brownian motion in the terms of translational and rotational diffusion, the particle dimensions can be determined by the decay rates of the fluctuations of the scattered light. Decay rates are determined for the light scattered with two different polarizations, one of which (copolarization) aligns with the polarization of the exciting light (VV, polarization angle 0°), and the other (cross-polarization) is perpendicular to it (VH, polarization angle 90°). The intensity autocorrelation functions (ACF) $G^{(2)}_{VV}(\tau)$ and $G^{(2)}_{VH}(\tau)$, where τ is the ACF delay time, are calculated from the time dependences of the scattered light intensity. These ACFs are related to the nanoparticles translational and rotational diffusion coefficients D_{trans} and D_{rot} . The particle length L and diameter d can be found from the values of the diffusion coefficients using the diffusion model for particles of a given shape (e.g., cylindrical). Moreover, measurements conducted at different polarization angles lead to more precise results in the determination of rod dimensions [14]. Depolarized DLS measurements have already been used for determination of the size parameters of Au nanorods and carbon

nanotubes [16,17]. Wide application of depolarized DLS to nonspherical nanoparticle characterization is limited at the moment because of challenges in measuring typically weak cross-polarized scattering signals and by the difficulties in analysis of experimental ACFs of the scattered light to determine the real dimensions of nanoparticles.

For calculating the length L and diameter d from the diffusion coefficients a diffusion model for particles in a solution is needed. Typically, equations for the coefficients of the translational and rotational diffusion can be reduced to the form

$$D_{trans} = \frac{kT}{3\pi\eta L} [\ln P + C_{trans}(P)]$$

$$D_{rot} = \frac{3kT}{\pi\eta L^3} [\ln P + C_{rot}(P)]$$

where k is the Boltzmann constant, T is the absolute temperature in K, η is the dynamic viscosity of the solvent, $P = L/d$ is the aspect ratio of the particle, C_{trans} and C_{rot} are the (aspect-ratio dependent) correction factors for the translational and rotational diffusion, respectively, that take into account the finite length effects at the ends of the cylinder. Different theories describing the diffusion of cylindrical particles in a liquid give different correction factors. In the simplest case $C_{trans} = C_{rot} = 0$, and the model reduces to the classical theory of Kirkwood, that was also used by [14] for analysis of the gold nanorod solutions and the same model was applied in the case of our study. The formulas that take into account cylinder end effects are different in different models (however, in almost all models C_{trans} and C_{rot} can be considered as functions of the inverse aspect ratio $1/P$) and in addition to that, the rod shape is in most cases different from an ideal cylinder. Therefore, precise calculation of size parameters from the translational and rotational diffusion coefficients by means of theoretical modelling seems to be rather complicated.

Despite the difficulties related with this method we decided to apply it to our samples and made MP DLS measurements of samples IL26 (as a starting sample), A4 and S1 (samples after successful ligand exchange with PEG-SH). D_{trans} and D_{rot} were calculated from different sets of polarization angles in order to find the combination which results in the smallest ACF approximation error, which was calculated according to formula below [14]:

$$\delta = \frac{\sum_{i=1}^N [G_{exper}(\tau_i) - G_{calc}(\tau_i)]^2}{\lim_{\tau \rightarrow \infty} G_{calc}(\tau)}$$

Examples of the experimental ACFs with corresponding fits using the fitting procedure from [14] can be found in Figure 5.

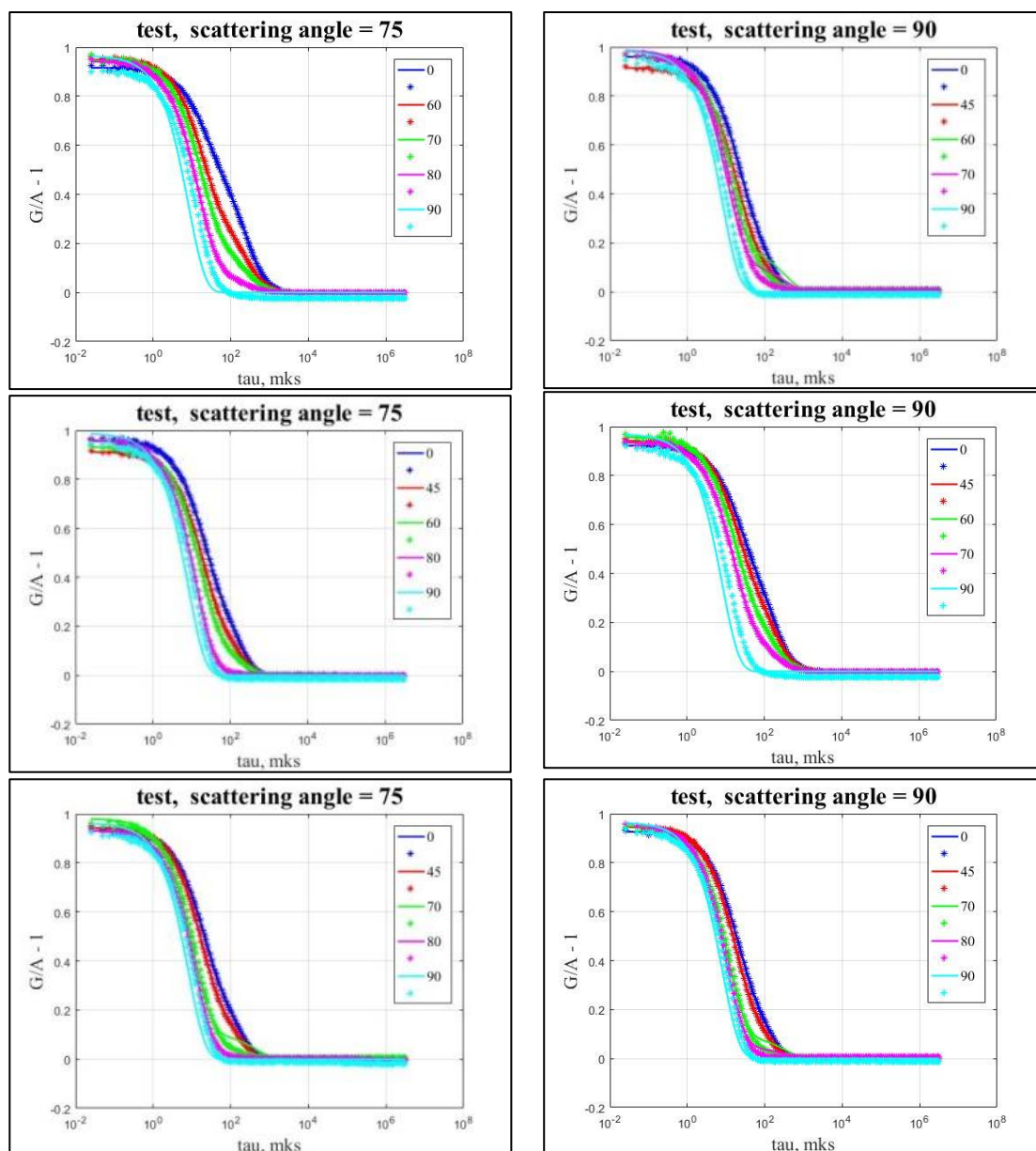


Figure 5. Series of MP DLS measurements at different angles between incident and scattered polarizations at a fixed scattering angle.

Different series of ACFs were analyzed to obtain the D_{rot} and D_{trans} coefficients. It was found that the set of polarization angles [0,45,60] in all cases led to the smallest mistake δ (see above) and these data for all samples under study can be found in Table 3.

Table 3. Results from DLS measurements for samples IL26 (CTAB-stabilized Au NRs) and S1 (PEG-coated Au NRs, scattering angle 90°, polarization angles 0°,45°,60°)

Sample	$D_{\text{trans}}, \mu\text{m}^2\text{s}^{-1}$	$D_{\text{rot}}, \text{ms}^{-1}$	length, nm	diameter, nm	aspect ratio
IL26	9.00	6.88	108.5±4.0	15.2±0.6	7.1
S1	9.06	7.40	104.9±3.4	15.5±0.5	6.8

Comparison of DLS parameters for S1 and the initial sample IL26 shows almost no difference. This oddity might be interpreted as imperfection of the model used for calculation of the nanorod dimensions from the coefficients of the translational and rotational diffusion. Presumably, assumption of coefficients $C_{trans}(P)$, $C_{rot}(P)$ being neglected is not acceptable and other expressions should be used. Authors of the method [14] also faced this inaccuracy, i.e. the comparison of obtained DLS data with TEM and UV-VIS results showed substantial difference between them.

The obtained length and width from DLS for the initial sample IL26 were further compared with the results obtained from TEM and UV-VIS data, which are summarized in Table 4. Nanorod aspect ratio P was also estimated from the values of the peak wavelength λ_{LSPR} using the formula from [18]:

$$P = 0.0098 \cdot \lambda_{LSPR} - 4.12, \text{ where } \lambda_{LSPR} \text{ is in nanometers.}$$

Table 4. Comparison of nanorod parameters for sample IL26 obtained from MP DLS, TEM and UV-VIS data

length, nm			diameter, nm			Aspect ratio		
MP DLS	TEM	L_{DLS}/L_{TEM}	MP DLS	TEM	d_{DLS}/d_{TEM}	MP DLS	TEM	UV-VIS
108.5±4.0	73.6± 7.8	1.47	15.2±0.6	20.1±2.6	0.75	7.1	3.7	4.1

Whereas the aspect ratio obtained from TEM and absorption spectroscopy is quite similar, the DLS seems to overestimate the aspect ratio substantially. This leads to the conclusion that the assumption that the coefficients $C_{trans}(P)$, $C_{rot}(P)$ can be neglected is not acceptable and one should take into account the aspect ratio dependence of these coefficients.

5. Purification procedure of non-monodisperse Au nanorod sample

During my summer project another task was to study the purification procedure of non-monodisperse sample of Au nanorods. Even though there are a lot of synthetic methods that are declared as “syntheses of monodisperse samples” [1] sometimes the resulting Au nanoparticles exhibit other shapes besides nanorods (especially for high aspect ratio samples). That is why it is desirable to establish the purification procedure which would remove all undesirable shapes and increase the monodispersity of the sample.

5.1 Experimental part

The sample of IL28 Au NRs was synthesized previously according to [1], method 3i. After synthesis it was purified once (centrifuged at 7000 rpm for 30 min, redissolved in 10 ml water).

Purification was based on a modified version of the method reported by Jana[19]. Typically, the synthesized solution of Au NRs is centrifuged, the dark precipitate is collected from each centrifuge tube and the supernatant is discarded. All the precipitates collected from the starting solution are dissolved in 40 mL of 0.3 M hot (40–50 °C) CTAB solution. After slow cooling process at room temperature (to avoid crystallization of CTAB due to supersaturation) a brown precipitate along with a pink supernatant can be observed. The precipitate is separated from the supernatant and again redissolved in a fresh portion of 40 mL of 0.3 M hot CTAB solution and left for cooling. This precipitation and redispersion can be repeated many times, typically 4–5 times for the complete separation of long rods.

10 ml of the initial sample was divided in two parts. Sample 1 (5 ml of stock solution) was purified with 0.1M CTAB solution, later centrifuged and purified twice with 0.3M CTAB, after that excess CTAB was removed by cleaning with water 3 times. Sample 2 (5 ml of stock solution) was purified with 0.3M CTAB solution three times, after that cleaned with water 3 times.

5.2 Results and discussion

Analysis of the TEM images of the initial sample led us to the conclusion that sample is not monodisperse and a large amount of particles with other shapes could be found (Fig.6)

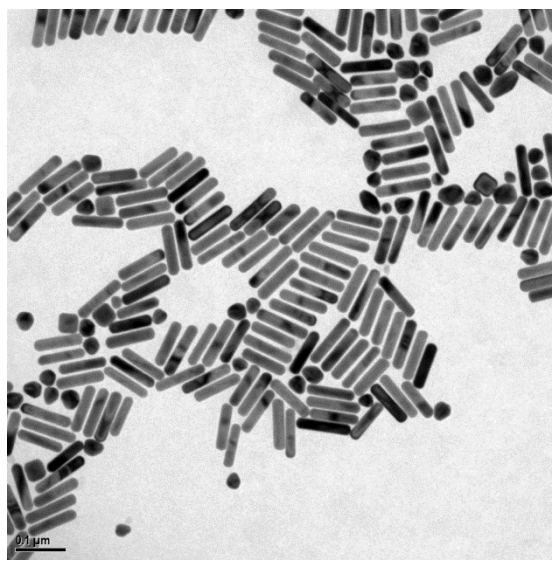


Figure 6. TEM image of as-synthesized IL28 Au NRs; non-rodlike particles can be seen here.

After the abovementioned purification procedure sample 1 was destroyed because of the aggregation. The reason was removal of too much CTAB due to the multiple precipitation of the particles, whereas sample 2 seemed to be a clean solution of Au nanorods.



Figure 7. Supernatant 2 for sample 2(left) and supernatant 1 for sample 1 (right). Bright pink color indicates spherical particles in the solution.

UV-VIS-NIR spectra of supernatants in different purification steps were measured. As it can be seen from Figure 8 for sample 1, the first supernatant (C1-1) contained nearly all non-rodlike particles whereas the second supernatant (C1-2) contained mainly rods which indicates that one step of purification is essential to remove the majority of non-rodlike particles. However, the absorbance at higher wavelengths for the product spectrum (C1-P) indicates the particle aggregation.

UV-VIS-NIR spectra for sample 2 show similar trend. First supernatant (C3-1) containing the main part of non-rodlike particles and the other supernatants (C3-2,3) containing rodlike particles due to inaccurate extraction. The spectrum of the final product (C3-P, the precipitate redissolved in water) indicates that some aggregation also occurred. However, due to the bigger amount of CTAB added in the purification process the purified solution of Sample 2 seems to be more stable after washing with water.

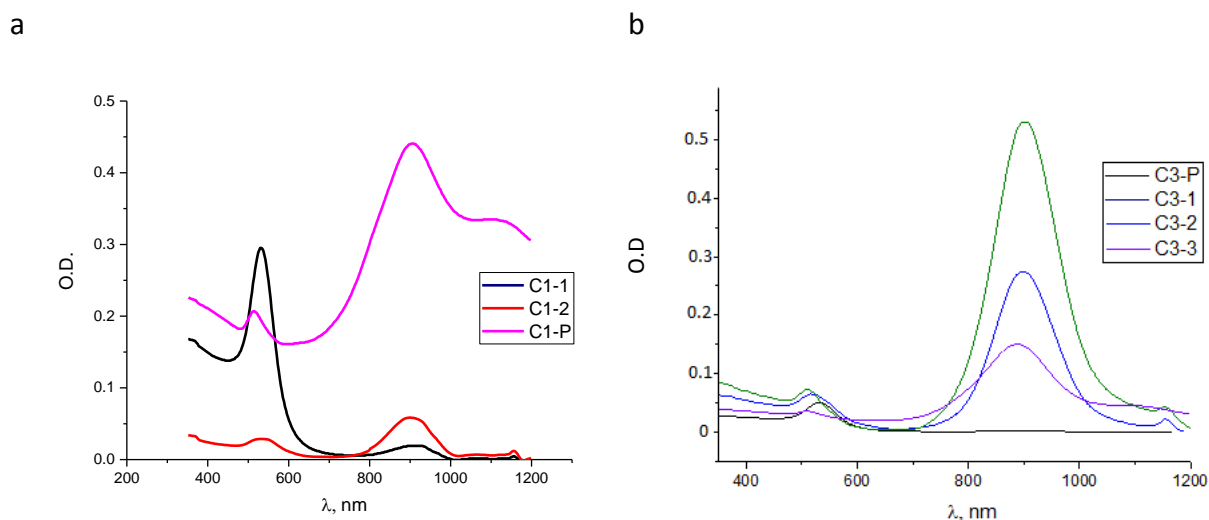


Figure 8. a) Absorption spectra of Sample 1, where C1-P is product and C1-1,2 are supernatants 1,2 respectively b) Absorption spectra of Sample 2, where C3-P is product and C3-1,2,3 are supernatants 1,2,3 respectively

Analysis of TEM images of the sample 2 after the purification showed that the concentration of non-rodlike particles decreased significantly, but there are still some of them in the solution (Figure 9)

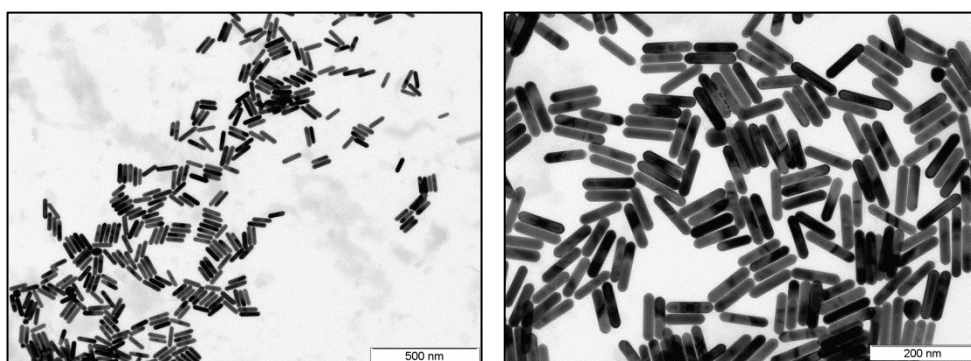


Figure 9. TEM images of the Sample 2 after purification procedure.

In conclusion, this type of purification does not allow us to remove all the spherical nanoparticles from the solution of Au nanorods, even though their concentration is significantly decreased. Furthermore, it has to be noted that one should be careful with washing of the samples after purification in order to remove excess CTAB with water, because addition of too much water may cause particle aggregation afterwards due to removal of too much CTAB needed for the stabilization of the particles.

6. Conclusions

During the summer project at DESY in the FS-CXS group we were investigating the properties of Au nanorods in colloidal solutions. The part of my work involved the surface modification of as-synthesized CTAB-coated Au NRs with methoxy-PEG-thiol ligands. Different methods of PEGylation were tested, several PEGylated samples were obtained and studied by means of different analytical methods. The stability of PEGylated Au nanorods dispersions in the high ionic strength media and tendency to dissolve both in organic and inorganic solvents were observed. The successful ligand exchange was demonstrated by UV-VIS-NIR spectroscopy, where PEG-coated Au NRs solutions exhibit stability upon addition of KCl compared to CTAB-stabilized nanorods.

The nanorods before and after ligand exchange with PEG were characterized by means of MP DLS method reported recently [14]. The calculation of translational and rotational diffusion coefficients from DLS data obtained for different polarization angles at a fixed scattering angle was used to determine the length and width of Au NRs. Whereas the length of Au NRs was comparable with that obtained from TEM, the width of Au NRs from DLS was substantially underestimated. Moreover, the purification procedure of non-monodisperse sample was carried out. Additionally, we developed a semi-automatic algorithm for the TEM image analysis using ImageJ freeware. It allows for determination of length and width of a large amount of Au NRs.

Development of efficient DLS and TEM analysis of anisotropic particles within colloidal solutions is essential for their processing and is an intriguing topic of current and future investigations.

7. Literature references

1. Ye, X., Zheng, C., Chen, J., Gao, Y., & Murray, C. B. (2013). Using binary surfactant mixtures to simultaneously improve the dimensional tunability and monodispersity in the seeded growth of gold nanorods. *Nano letters*, 13(2), 765-771.
2. Scarabelli, L., Sánchez-Iglesias, A., Pérez-Juste, J., & Liz-Marzán, L. M. (2015). A “tips and tricks” practical guide to the synthesis of gold nanorods.
3. Park, K., Biswas, S., Kanel, S., Nepal, D., & Vaia, R. A. (2014). Engineering the optical properties of gold nanorods: independent tuning of surface plasmon energy, extinction coefficient, and scattering cross section. *The Journal of Physical Chemistry C*, 118(11), 5918-5926.
4. Jain, P. K., Lee, K. S., El-Sayed, I. H., & El-Sayed, M. A. (2006). Calculated absorption and scattering properties of gold nanoparticles of different size, shape, and composition: applications in biological imaging and biomedicine. *J. Phys. Chem. B*, 110(14), 7238-7248.
5. Gómez-Graña, S., Hubert, F., Testard, F., Guerrero-Martínez, A., Grillo, I., Liz-Marzán, L. M., & Spalla, O. (2011). Surfactant (bi) layers on gold nanorods. *Langmuir*, 28(2), 1453-1459.
6. Kinnear, C., Dietsch, H., Clift, M. J., Endes, C., Rothen-Rutishauser, B., & Petri-Fink, A. (2013). Gold Nanorods: Controlling Their Surface Chemistry and Complete Detoxification by a Two-Step Place Exchange. *Angewandte Chemie International Edition*, 52(7), 1934-1938.
7. Takahashi, H., Niidome, Y., Niidome, T., Kaneko, K., Kawasaki, H., & Yamada, S. (2006). Modification of gold nanorods using phosphatidylcholine to reduce cytotoxicity. *Langmuir*, 22(1), 2-5.
8. Schulz, F., Friedrich, W., Hoppe, K., Vossmeier, T., Weller, H., & Lange, H. (2016). Effective PEGylation of gold nanorods. *Nanoscale*, 8(13), 7296-7308.
9. Abdelrasoul, G. N., Magrassi, R., Dante, S., d'Amora, M., d'Abbusco, M. S., Pellegrino, T., & Diaspro, A. (2016). PEGylated gold nanorods as optical trackers for biomedical applications: an in vivo and in vitro comparative study. *Nanotechnology*, 27(25), 255101.
10. Zhang, Z., & Lin, M. (2014). Fast loading of PEG-SH on CTAB-protected gold nanorods. *RSC Advances*, 4(34), 17760-17767.
11. BaniáYaseen, A. I. (2014). Facile phase transfer of gold nanoparticles from aqueous solution to organic solvents with thiolated poly (ethylene glycol). *RSC Advances*, 4(95), 52676-52679.
12. Zou, R., Guo, X., Yang, J., Li, D., Peng, F., Zhang, L., ... & Yu, H. (2009). Selective etching of gold nanorods by ferric chloride at room temperature. *CrystEngComm*, 11(12), 2797-2803.
13. Stevens, R., Stevens, L., & Price, N. C. (1983). The stabilities of various thiol compounds used in protein purifications. *Biochemistry and Molecular Biology Education*, 11(2), 70-70.

14. Levin, A. D., Shmytkova, E. A., & Khlebtsov, B. N. (2017). Multipolarization Dynamic Light Scattering of Nonspherical Nanoparticles in Solution. *The Journal of Physical Chemistry C*, 121(5), 3070-3077.
15. <https://imagej.nih.gov/ij/>
16. Glidden, M.; Glidden, M., & Muschol, M. (2012). Characterizing gold nanorods in solution using depolarized dynamic light scattering. *The Journal of Physical Chemistry C*, 116(14), 8128-8137.
17. Shetty, A. M., Wilkins, G. M., Nanda, J., & Solomon, M. J. (2009). Multiangle depolarized dynamic light scattering of short functionalized single-walled carbon nanotubes. *The Journal of Physical Chemistry C*, 113(17), 7129-7133.
18. Goodman, J. W. (2015). *Statistical optics*. John Wiley & Sons.
19. Jana, N. R. (2003). Nanorod shape separation using surfactant assisted self-assembly. *Chemical Communications*, (15), 1950-1951.

8. Acknowledgments

I would like to thank my supervisor Irina Lokteva for support, time spending and sharing the knowledge. Also I would like to thank all members of FS-CXS group for hosting me this summer and being so friendly. And, of course, I would like to thank all people who organized this wonderful summer programme. It was a great experience and unforgettable summer.